

DOI: 10.1002/cctc.201300457

TUD-1-Encapsulated HY Zeolite: A New Hierarchical Microporous/Mesoporous Composite with Extraordinary Performance in Benzylation Reactions

Mohamed S. Hamdy*^[a, b] and Guido Mul^[a]*Dedication: To Prof. Dr. Abd El-Hai Ebaid, the former president of Helwan University, Cairo, Egypt, on his retirement*

A new composite material consisting of amorphous TUD-1 encapsulating crystalline zeolite Y was synthesized. Samples with different HY zeolite loadings (10, 20, 40, and 60 wt%) were prepared, and the resulting solid products were characterized with elemental analysis, XRD, N₂ physisorption, ²⁷Al MAS NMR, IR, pyridine adsorption in combination with FTIR, temperature-programmed desorption of ammonia, HRSEM, and HRTEM. Characterization data confirm the presence of a thin layer of the mesoporous TUD-1 phase with a thickness of 30–100 nm

surrounding the zeolite crystals. The catalytic performance of the composite was studied in the Friedel–Crafts benzylation of benzene with benzyl alcohol at 353 K. The catalytic activity of the HY/TUD-1 composite was higher than that of HY zeolite, whereas the composite showed a much slower rate of deactivation. The improved performance of the composite is related to beneficial changes in the acidity of the HY crystal through chemical interactions with TUD-1.

Introduction

Zeolites are microporous crystalline aluminosilicates with well-defined structures.^[1] Zeolite Y is a highly versatile zeolite from the faujasite family, the 3 D pore structure and acidic characteristics of which have been used in various applications. However, although the micropores provide for a large internal surface area containing active sites, they induce resistance for mass transport to or from the active sites.^[2] In zeolite Y, mass transfer limitations can occur if large reactant molecules are involved.^[3,4] To overcome this problem, the synthesis of large-pore zeolites^[5,6] and zeolites consisting of nanosized crystals^[7,8] has been reported. However, owing to the low acidity and low thermal stability of the large-pore zeolites as well as the high pressure drop limiting the practical application of nanosized zeolites, an alternative catalyst design is needed.^[6]

Microporous/mesoporous composite materials with hierarchical pore structures seem to be promising because they combine both the catalytic features: the strong acidity of a microporous zeolite and improved access and transport properties of mesoporous materials.^[9,10] Synthetic methods for the preparation of microporous/mesoporous composite materials have already been reported.^[11,12] The synthesis of hierarch-

ical composites of zeolite Y incorporated in MCM-41,^[13,14] MCM-48,^[15] and SBA-15^[16] has been achieved. TUD-1^[17] is a well-established sponge-like mesoporous solid material. TUD-1 has many advantages compared to other mesoporous materials (e.g., MCM-41), such as a cost-effective synthesis (surfactant-free), a 3 D structure, a tunable pore size distribution, and a surface area reaching values of 900 m²g⁻¹.^[17] TUD-1 was used as a support for different metal ions or oxide particles, such as Ti,^[18] Mo,^[19] Cr,^[20] and Cu.^[21] Moreover, TUD-1 was used in a hierarchical composite with beta zeolite,^[22] ZSM-5,^[23] and ITQ-2.^[24] The beta zeolite/TUD-1 composite demonstrates improved performance compared to beta zeolite in the cracking of *n*-hexane^[22] and the cyclohydration of xylose.^[25]

In 2005,^[26,27] we reported the Friedel–Crafts benzylation of benzene over Fe-TUD-1. This bifunctional catalyst shows a unique activity, that is, 100% conversion within 90 seconds. However, leaching of Fe from the framework cannot be prevented and thus it hinders practical application. Herein, a new composite of zeolite Y and TUD-1 was prepared with different zeolite loadings. The prepared composite material was characterized extensively, and the catalytic performance was investigated in the liquid phase Friedel–Crafts benzylation of benzene. The activity and deactivation rate of HY/TUD-1 are compared with those of the parent HY catalyst, and the improved performance of the composite is discussed extensively.

[a] Dr. M. S. Hamdy, Prof. Dr. G. Mul
Faculty of Science and Technology
MESA⁺ Institute for Nanotechnology
Twente University, P.O. Box 217, 7500 AE Enschede (The Netherlands)

[b] Dr. M. S. Hamdy
Chemistry Department
Faculty of Science
Helwan University, 11795 Ein Helwan, Cairo, Egypt
Fax: (+20)225552467
E-mail: m.s.hamdy@gmail.com

Results and Discussion

Morphology of HY/TUD-1 catalysts

The XRD patterns of the prepared samples are compared with those of pure zeolite Y and TUD-1 in Figure 1. A diffraction line

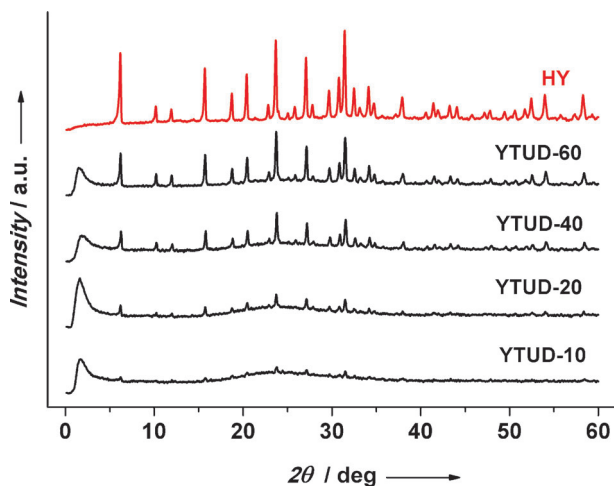


Figure 1. Powder XRD patterns of the prepared HY/TUD-1 samples compared with those of TUD-1 and HY zeolite used as references.

can be observed at a low angle of $2\theta = 1\text{--}2.5^\circ$ in the pattern of the composites, which is characteristic of mesoporous materials and indicates the presence of TUD-1. Furthermore, the XRD pattern shows the characteristic lines of zeolite Y with the increase in intensity, which increases with zeolite Y content. The similar width of the zeolite Y diffraction lines in various samples suggests a similar crystallite size in all samples. The diffraction line at low angle in the XRD pattern of TUD-1 corresponds to a short-range correlation of nuclear density at a distance of 4.5–5 nm. This line weakens, broadens, and shifts to larger angles with the increase in zeolite content, which implies that the short-range order is increasingly disrupted and that the remaining structure is heterogeneous in nature, that is, a less well-defined TUD-1 structure is obtained in the presence of HY.

Elemental analysis was used to calculate the Si/Al ratio in the HY/TUD-1 composite and hence to determine the amount of zeolite in the synthesized samples. The amount of zeolite detected in the final products is identical to the amount of zeolite added to the synthesis mixtures (Figure 2 and Table 1).

The N_2 adsorption–desorption isotherms of various HY/TUD-1 samples are presented in Figure 3a. According to IUPAC classification, the hysteresis loops of the prepared samples at a relative pressure of 0.4–0.9 show characteristic features of type IV isotherms, which are representative of mesoporous materials and also typical for TUD-1 materials.^[17] For TUD-1, the loop is relatively narrow because the adsorption and desorption branches are vertical and nearly parallel

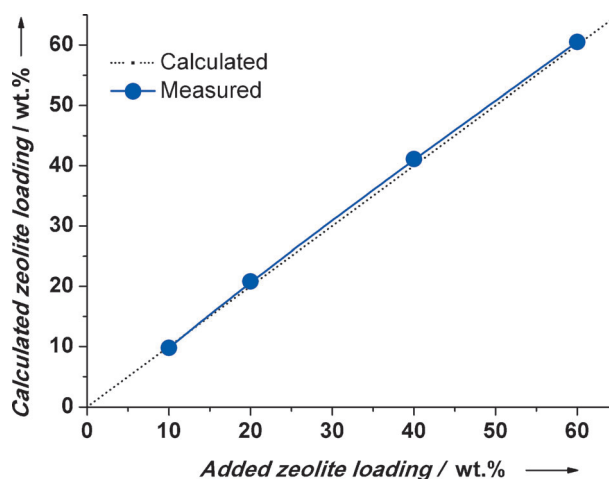


Figure 2. Correlation of the HY zeolite loading before (calculated) and after the synthesis of HY/TUD-1, which is based on the Si/Al ratio determined from elemental analysis.

(H1-type hysteresis loop). Owing to the incorporation of HY zeolite into the synthesis mixture of TUD-1, the hysteresis loops change and become broad because the desorption branch is steeper than the adsorption branch. The pore filling and emptying profile indicates the presence of a wide range of nonuniform pores (H3-type hysteresis loop) including mesoporosity. The adsorption–desorption isotherm of HY zeolite demonstrates a type I isotherm, in which N_2 uptake increases quickly at low relative pressure, which is characteristic of microporous materials. After monolayer adsorption at low relative pressure, N_2 uptake is constant and a small hysteresis loop at high relative pressure can be observed in the adsorption–desorption curves.^[28]

The corresponding BJH (BJH = Barrett–Joyner–Halenda) pore size distributions of the prepared samples compared to the HY zeolite sample are shown in Figure 3b. In general, the mesopore size increases with the increase in zeolite loading. Similar behavior was found for the beta zeolite/TUD-1 composite.^[22] The BET surface area and the external surface area are plotted as a function of zeolite loading in Figure 3c. The BET surface area of the prepared samples increases slightly with the increase in HY loading. However, the external surface area decreases sharply. This result reflects the contribution of TUD-1 (on a per-gram basis, $\approx 665\text{ m}^2$) to the external surface area relative to the contribution of the zeolite crystals

Table 1. Texture properties as determined from N_2 adsorption–desorption measurements.

Sample	Surface area		Average pore volume		Pore diameter [nm]
	BET [m^2g^{-1}]	External [m^2g^{-1}]	Mesopore [cm^3g^{-1}]	Micropore [cm^3g^{-1}]	
YTUD-10	597	597	0.74	0.314	5.14
YTUD-20	575	538	0.65	0.325	4.47
YTUD-40	654	400	0.62	0.311	6.40
YTUD-60	667	238	0.59	0.337	7.43
Pure HY	660	18	0.37	0.336	0.7

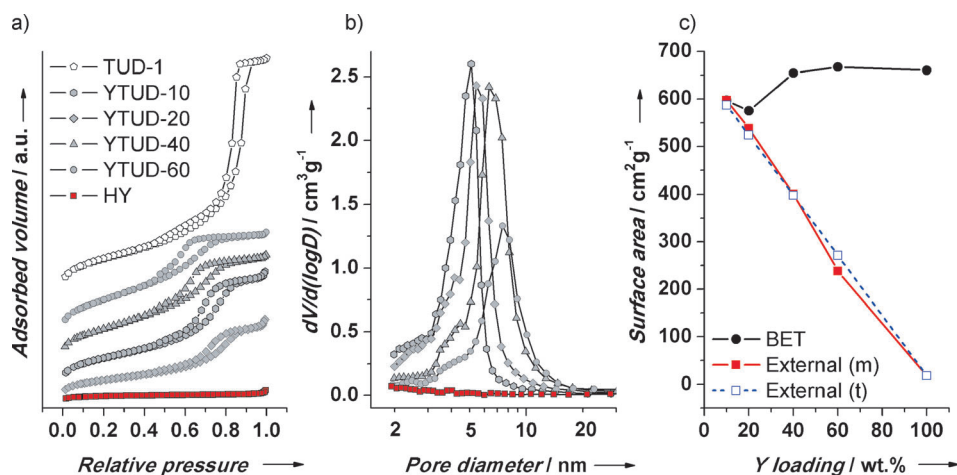


Figure 3. a) N₂ adsorption–desorption isotherms of the prepared HY/TUD-1 samples compared with those of TUD-1 and HY zeolite. b) The corresponding pore size distribution of HY/TUD-1 samples. c) The BET and the external surface areas (m = measured; t = theoretical) as a function of zeolite loading.

(18 m² g⁻¹). The consequent theoretical change is also shown in Figure 3, which confirms that the synthetically intended ratio of HY over TUD-1 was obtained. The small increase in BET area is due to the increasingly larger contribution of the internal surface area of the zeolite crystals.

The ²⁷Al MAS NMR spectra of HY zeolite and YTUD-40 sample are shown in Figure 4a. The spectra of both samples are dominated by an intensive peak at approximately 57 ppm, which indicates the presence of Al species in tetrahedral coordination. A small peak at approximately 0 ppm is also present, which is attributed to octahedrally coordinated Al, presumably reflecting the degree of hydration of the sample and possibly the presence of some extra framework Al atoms. The spectrum of HY is similar to that presented by Chang et al.^[29] The constant ratio between the two NMR signals suggests that the partial dissolution or loss of structure of the zeolite crystals during the formation of the TUD-1 matrix has not occurred.

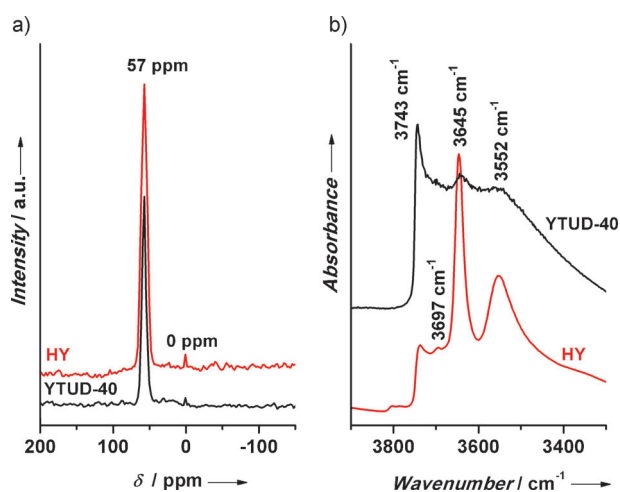


Figure 4. a) ²⁷Al MAS NMR spectrum of neat HY zeolite compared with that of the YTUD-40 sample. b) IR spectrum of HY zeolite compared with that of YTUD-40.

The IR spectra of YTUD-40 and neat HY zeolite are shown in Figure 4b. The IR spectrum of HY zeolite is dominated by three bands at approximately 3743, 3645, and 3552 cm⁻¹. In addition, a small band at approximately 3695 cm⁻¹ is observed. The bands at approximately 3645 and 3552 cm⁻¹ have been assigned to Brønsted acidity generated by the Si–OH–Al groups in the large supercages^[30] and in the sodalite cages,^[31] respectively. The band at approximately 3743 cm⁻¹ is attributed to silanol (Si–OH) groups. The band at approximately 3695 cm⁻¹ can be attributed to Al–OH groups associated with extraframework Al atoms, which is consistent with the ²⁷Al MAS NMR spectrum. All these bands are visible in the YTUD-40 sample, which is quite dominated by the silanol groups of the TUD-1 matrix. By summarizing the data of NMR and IR spectroscopy, one can conclude that the zeolite crystals did not undergo any change in phase composition or significant dealumination during or after the synthesis of the composite.

The temperature-programmed desorption of ammonia (NH₃-TPD) profiles of HY, YTUD-40, siliceous TUD-1, and a physical mixture consisting of 40% zeolite Y and 60% TUD-1 are shown in Figure 5a.

All profiles (except of TUD-1) are dominated by one broad peak at approximately 590 K, which is attributed to the desorption of NH₃ from strongly acidic sites.^[32] It is clearly observed that the number of acidic sites is much larger for the composite than for siliceous TUD-1 but smaller than for HY. The profiles of the physical mixture and YTUD-40 are not identical: the peak height of YTUD-40 is significantly smaller than that of the physical mixture of equal composition, which is due to the formation of new bonds between the surface of the zeolite crystals and the TUD-1 mesoporous material during the synthesis of the composite.

To quantify the number of Lewis and Brønsted acid sites in the prepared samples, pyridine adsorption in combination with FTIR spectroscopy was used (Figure 5b and Table 2). Lewis acid sites are usually identified by a band at 1445 cm⁻¹, whereas Brønsted acid sites result in a band at 1545 cm⁻¹.^[33] According to an earlier study,^[34] siliceous TUD-1 contributes significantly to the intensity at 1445 cm⁻¹ owing to Lewis acidity; however, TUD-1 has no Brønsted acidity. Thus, in the HY/TUD-1 composites, the Lewis acid band consists of two overlapping bands: the TUD-1 band and the HY band. The two bands decrease with the decrease in zeolite loading (Figure 5b), which is partly due to the decrease in the quantity of HY in the sample. However, the Brønsted acidity band decreases with a considerable deviation of the expected value based

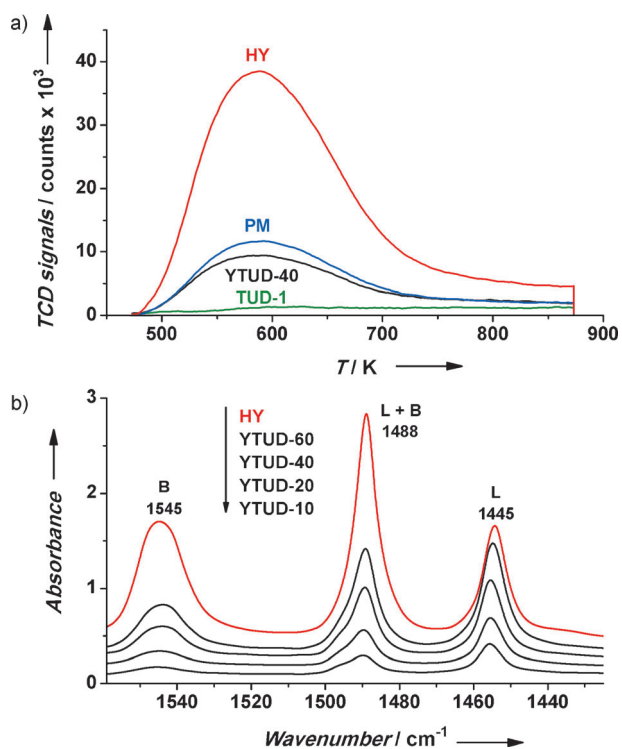


Figure 5. a) NH_3 -TPD profiles of YTUD-40 compared with those of TUD-1, HY zeolite, and a physical mixture (PM) with the same HY/TUD-1 ratio. b) Pyridine adsorption in combination with FTIR spectra of HY/TUD-1 samples compared with those of the parent HY sample.

on the weight fraction. The deviation is indicated in Table 2, which ranges between 26 and 36%. This deviation is due to the formation of new chemical bonds between the zeolite crystals and the TUD-1 mesoporous material. Furthermore, such a high deviation ratio is an indication that Brønsted acid sites are converted not only on the external surface of the HY crystals by covering with TUD-1 but also in the pore system of the zeolite crystals.

HRSEM was used to study the particle shape and morphology of the prepared samples. The micrographs of YTUD-10 and YTUD-60 samples are shown in Figure 6. The YTUD-10 micrograph (Figure 6a) shows a homogeneous morphology of the sample that is assigned to the TUD-1 matrix. Zeolite crystals are not apparent. However, with the increase in zeolite load-

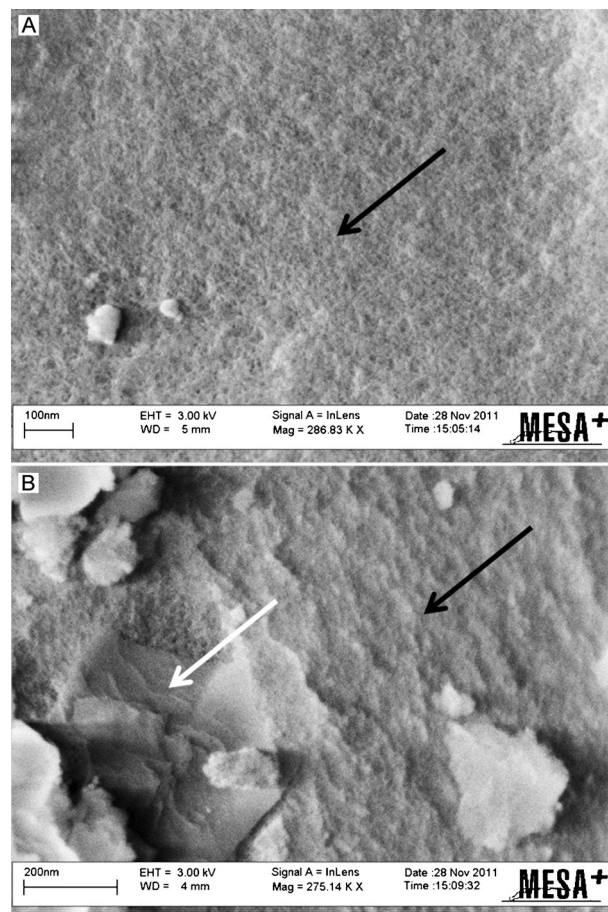


Figure 6. HRSEM micrographs of A) YTUD-10 and B) YTUD-60. The white arrows point to the zeolite crystals, whereas the black arrows point to the TUD-1 mesoporous matrix.

ing, zeolite crystals become visible (Figure 6b) and the overall composite structure is not as homogeneous.

The HRTEM micrographs of the YTUD-40 sample are shown in Figure 7, which demonstrate a thin layer of mesoporous material encapsulating the zeolite crystals. The thickness of the mesoporous layer was estimated to be 30–100 nm. The zeolite crystals seem to be largely covered; however, the agglomeration of zeolite crystals was not observed.

Catalytic performance of HY/TUD-1

The catalytic activity of different HY/TUD-1 samples was evaluated in the liquid phase Friedel–Crafts benzylation of benzene. The reactions were performed at 353 K by reacting benzyl alcohol with an excess of benzene. Diphenylmethane was the major product detected in all the reactions, with a selectivity of greater than 90%. Other products such as dibenzylether were only minor in quantity (selectivity > 10%). This result is in agreement with the results of Coman et al.^[35] and Chaube.^[36]

The rate data (time-dependent benzyl alcohol conversion data) of the benzylation reaction of benzene

Table 2. Acidity of HY/TUD-1 samples compared with the parent HY as determined by pyridine adsorption in combination with FTIR measurements.

Sample	Brønsted acid sites [$\mu\text{mol g}^{-1}$] ^[a]			Lewis acid sites [$\mu\text{mol g}^{-1}$]	Brønsted/Lewis acid ratio
	Exp	Calcd	Diff [%]		
YTUD-10	19.5	29.2	33	50.9	0.38
YTUD-20	43.4	58.4	26	80.9	0.54
YTUD-40	86.9	116.9	26	128.8	0.67
YTUD-60	110.9	175.3	36	181.3	0.61
Pure HY	292.1	–	–	172.3	1.7

[a] Exp = measured value; Calcd = calculated value; Diff = difference between the calculated and the measured Brønsted acidity.

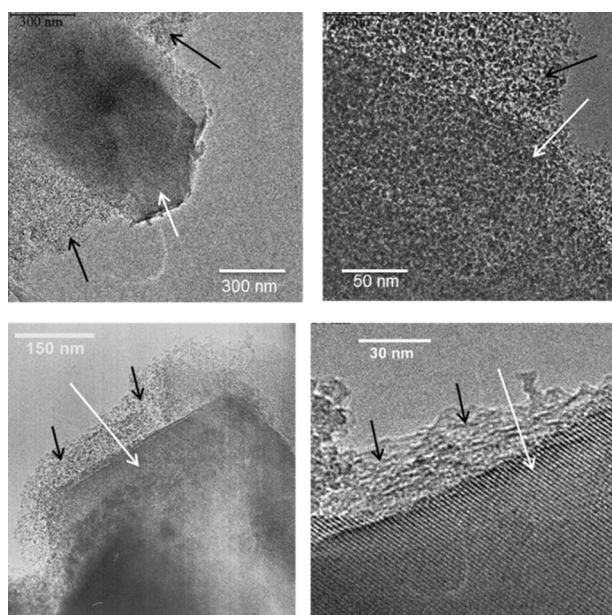


Figure 7. HRTEM micrographs of the YTUD-40 sample. The white arrows point to the zeolite crystals, whereas the black arrows point to the TUD-1 mesoporous matrix. The micrographs clearly show the formation of a thin layer of TUD-1 mesoporous material around the zeolite HY crystals.

with the HY/TUD-1 catalysts could be fitted well to a pseudo-first-order rate law. The apparent first-order rate constants of the different HY/TUD-1 samples, corrected for the amount of zeolite per gram of composite, are depicted in Figure 8. The rate of the reaction was negligible in the absence of the catalyst. As expected, TUD-1 did not show any conversion of benzyl alcohol. All HY/TUD-1 samples generally showed a higher reaction rate than neat HY zeolite, of which YTUD-40 showed the highest activity. YTUD-40 also showed higher ac-

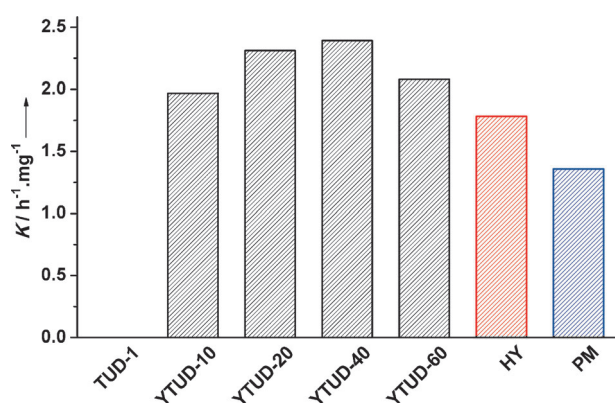


Figure 8. The apparent first-order rate constant of different catalysts applied in this work.

tivity compared to the physical mixture of HY and TUD-1. These results confirm the synergy between the zeolite crystals and TUD-1 in the composite. Shan et al.^[22] and Valente et al.^[25] observed a similar synergy between beta zeolite and TUD-1, even though in different catalytic applications.

The performance of YTUD-40 is compared with that of HY zeolite in Figure 9. HY zeolite continuously deactivates, with only 22% of its original activity remaining in the fourth run. The YTUD-40 sample demonstrates a much smaller rate of deactivation, losing only 10% of its original activity in three runs. In the fourth run, the activity of YTUD-40 was 5 times higher than that of HY zeolite.

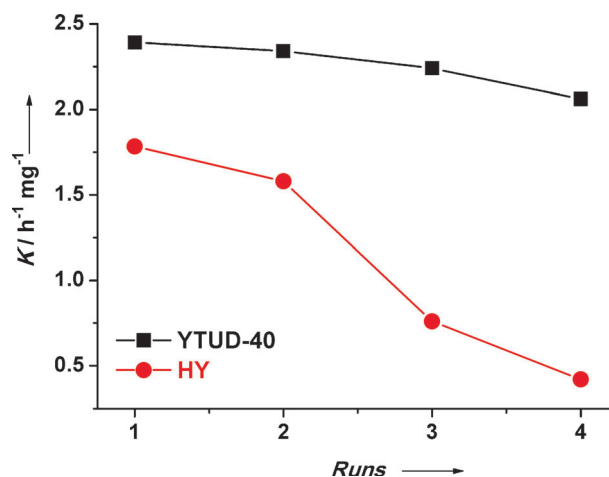


Figure 9. The apparent first-order rate constant of YTUD-40 compared with that of HY as a function of the number of runs.

TUD-1 was reported previously to accommodate several metal oxide nanoparticles, such as TiO_2 ,^[18] Cr_2O_3 ,^[20] and Fe_2O_3 .^[26] The size of those nanoparticles matched the mesopore size of the host, that is, siliceous TUD-1, which is consistent with the fact that those nanoparticles were formed inside the pores during the synthesis. However, in the case of pre-existing zeolite crystals, the TUD-1 silica matrix was reported to encapsulate (grow over) zeolite nanoparticles such as in the case of a beta zeolite/TUD-1 composite. Although the size of the beta zeolite nanoparticles is smaller (≈ 40 nm) than that of the zeolite Y nanoparticles (≈ 250 nm) used herein, the TEM micrographs of Figure 7 indicate the encapsulation of zeolite Y by TUD-1. This result demonstrates that well-defined zeolite/TUD-1 composites can be synthesized, irrespective of the particle size of the parent zeolite.

Several research groups have assigned improved performance of zeolite/mesoporous material composites to a smaller degree of agglomeration of the zeolite crystals, which could improve the accessibility of the active sites. However, if the time required for the reaction and the time required for diffusion are compared, it is found that the interparticle porosity of zeolite crystals most likely does not cause any mass transfer limitations (the Thiele modulus is close to zero). Hence, the beneficial effect of the encapsulation of the zeolite crystals by TUD-1 on activity and especially on stability observed herein must have a different origin.

It has been proposed that the mesoporous material could act as a "sponge."^[24,37] The mesoporous material could pre-concentrate the substrate, making it available for the dominant active (acidic) sites on the surface of the zeolite crystals. Al-

though we cannot exclude the sponge effect, which could be responsible for the improvement in activity, another factor is more apparent.

The most important property of the materials for the catalysis investigated is acidity. Generally speaking, Friedel–Crafts reactions cannot be catalyzed by weak Lewis acid sites of pure silica materials,^[33] such as MCM-41,^[38] SBA-15,^[39] and TUD-1.^[26] However, the Friedel–Crafts benzylation of benzene can be catalyzed by silica-based catalysts, either pure Lewis acids such as $\text{AlCl}_3/\text{MCM-41}$ or pure Brønsted acids such as Nafion-embedded silica.^[35] Furthermore, it has been reported that there is a synergy between Lewis and Brønsted acid sites with an appropriate ratio,^[40] that is, from 0.7 to 1 Brønsted/Lewis ratio.

In the HY/TUD-1 composite, the NH_3 -TPD and pyridine adsorption in combination with FTIR studies indicate that the mesoporous matrix reduces the total number of Brønsted acid sites of zeolite Y, probably by forming new bonds between the zeolite and the silica matrix of TUD-1. Thus, the Brønsted/Lewis ratio changes from 1.7 in the parent HY to 0.67 in YTUD-40, which is close to the optimized ratio reported previously. Thus, the overall reaction rate of the HY/TUD-1 composite per zeolite amount is higher than that of the parent HY (Figure 8).

Furthermore, the changes in acidity are in agreement with the reduction in the rate of deactivation of the composite compared to the parent HY zeolite.^[41] Zeolite Y deactivates sharply in liquid phase hydrocarbon reactions even at mild temperatures, which is due to coke formation.^[42–44] We thus suggest that the main benefit of the thin, highly porous TUD-1 layers (ensuring accessibility to the HY surface) in the performance of HY zeolite in benzylation reactions is the inhibition of a considerable number of strongly Brønsted acid sites, which prevents coke formation and zeolite deactivation. This suggestion is in agreement with the work of Dong et al.^[45] and Weckhuysen et al.,^[46] in which Brønsted acid sites are reported to be responsible for coke formation on the surface of zeolites.

This effect has also been observed in studies combining beta zeolite and TUD-1^[22,25] as well as ITQ-2 and TUD-1.^[24] Detailed IR studies of the beta zeolite/TUD-1 composites have shown that hydrogen bonded silanols are more dominant in the composite materials compared to TUD-1. Furthermore, the composite with approximately 40% beta zeolite contained the highest number of acid sites with medium acidity, which coincided with the highest activity in the cracking of *n*-hexane.^[24]

Conclusions

HY/TUD-1 composites were prepared by adding commercial HY zeolite to the synthesis mixture of the TUD-1 mesoporous material. The characterization data indicate the formation of a thin layer of the 3D TUD-1 matrix surrounding the zeolite crystals. The catalytic activity of HY/TUD-1 was higher than that of commercial HY zeolite in the Friedel–Crafts benzylation of benzene at 353 K. Furthermore, HY/TUD-1 showed improved stability compared to the parent HY zeolite. The improved performance of the composite is likely related to beneficial changes in the acidity of the HY crystals through encapsulation by TUD-1.

Experimental Section

Materials

The following chemicals were obtained and used without further treatment: tetraethyl orthosilicate (TEOS, > 98%, Acros Organics), triethanolamine (TEA, 97, Acros Organics), tetraethylammonium hydroxide (TEAOH, 35%, Aldrich), benzene (anhydrous, 99.8%, Sigma–Aldrich), and benzyl alcohol (anhydrous, 99.8%, Sigma–Aldrich). Zeolite Y (CBV-600) with a Si/Al ratio of 5.2 and crystal size around 250 nm was obtained from Zeolyst.

Synthesis

Four samples of the HY zeolite/TUD-1 composite were prepared by adding commercial zeolite Y to the synthesis mixture of TUD-1. The samples were labeled YTUD-*x*, with *x* representing a weight percentage of 10, 20, 40, or 60% of HY zeolite. In a typical synthesis method, deionized water was added to TEA and the mixture was shaken by hand for a few minutes until a pale yellow mixture was obtained. Then, TEOS was added dropwise with stirring. A suspension of zeolite Y in NH_3 (to avoid aggregation of the zeolite crystals) was added to the previous mixture under vigorous stirring. Finally, tetraethylammonium hydroxide was added dropwise. The obtained mixture was stirred until gelation. The final synthesis mixture has a molar ratio composition of $\text{SiO}_2/\text{TEA}/\text{TEAOH}/\text{H}_2\text{O} = 1:1:0.5:11$. The obtained gel was aged at RT for 24 h and then dried at 371 K for another 24 h. The obtained solid was gently ground, hydrothermally treated in a 50 mL Teflon-lined stainless steel autoclave at 451 K under autogenous pressure for 4 h, and finally calcined at 873 K for 10 h (heating rate: 1 K min^{-1}) in static air.

Characterization

Powder XRD patterns were measured with a Philips PW-1840 X-ray diffractometer equipped with a graphite monochromator using $\text{CuK}\alpha$ radiation ($\lambda = 0.1541 \text{ nm}$). The samples were scanned at $2\theta = 0.1\text{--}80^\circ$ with steps of 0.02° . Instrumental neutron activation analysis was used for the determination of the chemical composition at the THER nuclear reactor at the Delft University of Technology, with a thermal power of 2 MW and a maximum neutron flux of $2 \times 10^{17} \text{ m}^{-2} \text{ s}^{-1}$. The N_2 adsorption–desorption isotherms were recorded on a Quantachrome's AUTOSORB-6B at 77 K. Samples were evacuated previously at 623 K for 16 h. The pore size distribution was calculated from the adsorption branch by using the BJH model. The BET method was used to calculate the surface area of the samples, whereas the mesopore volume and external surface area were calculated by using the t-plot method.²⁷ ^{27}Al MAS NMR experiments were performed at a magnetic field of 9.4 T on a Varian VXR 400 S spectrometer operating at 104.2 MHz with a pulse width of 3.2 ms; 4 mm zirconia rotors were used, with the spinning speed set to 8 kHz. The chemical shifts were determined by using TMS as an external standard and set to 0 ppm. A total of 1000 scans were collected by using a sweep width of 20000 Hz and an acquisition delay of 20 s. The IR spectra were recorded on a Bio-Rad 176C spectrophotometer. Thin wafers of the samples (weighing $\approx 15 \text{ mg}$) were prepared by using a SPECTA press and applying a pressure of 3 tons cm^{-2} . Samples were mounted on a Cu sample holder equipped with a resistive heating element and a type K thermocouple. All samples were activated at 800 K for 4 h in air before spectral collection by averaging 200 scans at 8 cm^{-1} resolution. NH_3 -TPD was performed on a Micromeritics TPR/TPD 2900 apparatus equipped with a thermal conductivity detector.

The sample (30 mg) was pretreated at 787 K under He flow (flow rate: 30 mL min⁻¹) for 1 h. Then, pure NH₃ (flow rate: 40 mL min⁻¹) was adsorbed at 393 K for 15 min. Subsequently, He flow (flow rate: 30 mL min⁻¹) was passed through the reactor for 30 min to remove any weakly adsorbed NH₃ from the sample. The desorption of NH₃ was monitored in the range of 450–850 K (heating rate: 10 K min⁻¹). The pyridine in combination with FTIR spectra were recorded on a Nicolet 6700 FTIR spectrometer with a mercury cadmium telluride detector using the empty cell as a background, and collecting 128 scans with a resolution of 4 cm⁻¹. The catalyst (50 mg) was pressed into a wafer (diameter: 1.5 cm) by applying 2 ton to 1.767 cm² for 5 seconds. The sample was guided in a holder and placed in a homemade vacuum transmission cell specially designed for pyridine experiments. The samples have been outgassed by heating the sample (ramp rate: 1 K min⁻¹) at 393 K for 2 h and then at 673 K for another 2 h under vacuum of 2 × 10⁻⁵ mbar. Pyridine vapor was dosed in steps through a known volume and pressure until saturation. The samples needed to be heated till 433 K to diffuse pyridine inside and reach the acid sites. The last step is evacuation at 433 K in high vacuum to obtain the desired last unsaturated spectra. The HR-SEM micrographs were recorded at 30 kV on a LEO 1550 microscope equipped with NORAN electron-dispersive spectroscopy (EDS) and wavelength-dispersive spectroscopy (WDS). HR-TEM was performed on a Philips CM30UT electron microscope with a field emission gun as the source of electrons operated at 300 kV. Samples were mounted on a Cu-supported carbon polymer grid by placing a few droplets of a suspension of the ground sample in ethanol on the grid, followed by drying at ambient conditions.

Catalytic activity test

The liquid phase Friedel–Crafts benzylation reaction with HY/TUD-1 catalysts was performed in a magnetically stirred round bottom flask fitted with a reflux condenser and immersed in a temperature-controlled oil bath. In a typical reaction, the catalyst (0.1 g, which had been treated overnight in static air at 453 K) was introduced into the reaction flask and heated for 2 h at 393 K in vacuum. Subsequently, the flask was cooled down to the desired temperature and filled with dried N₂ gas. Then, benzene (10 mL, dried over molecular sieve) was added and stirred with the catalyst for a few minutes. Finally, benzyl alcohol (1.0 g, dried over molecular sieve) was added. Liquid samples were withdrawn at regular intervals and analyzed with a Varian Star 3500 gas chromatograph with a Sil 5 CB capillary column (50 m length, 0.53 mm inner diameter). All reactions were performed at least twice under identical conditions, and mass balances were closed within 97%. After the experiment, the catalyst was filtered and treated as reported in Ref. [39] at 393 K before reuse in a subsequent catalytic cycle.

Acknowledgements

We greatly acknowledge Ing. Mark Smithers, Twente University, for HRSEM micrographs and Dr. P. J. Kooyman, Dr. J. Groen, and B. van der Linden, Delft University of Technology, for HRTEM micrographs, N₂ sorption, and pyridine adsorption in combination with FTIR measurements, respectively.

Keywords: benzylation · Friedel–Crafts · heterogeneous catalysis · microporous/mesoporous composites · zeolites

- [1] H. Ghobarkar, O. Schäf, U. Guth, *Prog. Solid State Chem.* **1999**, *27*, 29–73.
- [2] J. van den Bergh, J. Gascon, F. Kapteijn, *Diffusion in Zeolites—Impact on Catalysis, Zeolites and Catalysis*, Wiley-VCH, Weinheim, **2010**, pp. 361–387.
- [3] C. Ercan, F. M. Dautzenberg, C. Y. Yeh, H. E. Barner, *Ind. Eng. Chem. Res.* **1998**, *37*, 1724–1728.
- [4] R. Rungtirsakun, T. Nanok, M. Probst, J. Limtrakul, *J. Mol. Graphics Modell.* **2006**, *24*, 373–382.
- [5] J. Coronas, *Chem. Eng. J.* **2010**, *156*, 236–242.
- [6] J. Jiang, J. Yu, A. Corma, *Angew. Chem.* **2010**, *122*, 3186–3212; *Angew. Chem. Int. Ed.* **2010**, *49*, 3120–3145.
- [7] M. A. Cambolor, A. Corma, A. Martínez, F. A. Mocholí, J. P. Pariente, *Appl. Catal.* **1989**, *55*, 65–74.
- [8] A. J. H. P. van der Pol, A. J. Verduyn, J. H. C. van Hooff, *Appl. Catal. A* **1992**, *92*, 113–130.
- [9] A. Corma, *Chem. Rev.* **1997**, *97*, 2373–2420.
- [10] K. Egeblad, C. H. Christensen, M. Kustova, C. H. Christensen, *Chem. Mater.* **2008**, *20*, 946–960.
- [11] J. C. Groen, L. A. A. Peffer, J. A. Moulijn, J. Pérez-Ramírez, *Chem. Eur. J.* **2005**, *11*, 4983–4994.
- [12] G. Zhu, S. Qiu, F. Gao, D. Li, Y. Li, R. Wang, B. Gao, B. Li, Y. Guo, R. Xu, Z. Liu, O. Terasaki, *J. Mater. Chem.* **2001**, *11*, 1687–1693.
- [13] Y. Wang, D. Cui, Q. Li, *Microporous Mesoporous Mater.* **2011**, *142*, 503–510.
- [14] T. Jiang, L. Qi, M. Ji, H. Ding, Y. Li, Z. Tao, Q. Zhao, *Appl. Clay Sci.* **2012**, *62–63*, 32–40.
- [15] Y. Zhang, Y. Liu, Y. Li, *Appl. Catal. A* **2008**, *345*, 73–79.
- [16] X. Zhang, F. Zhang, X. Yan, Z. Zhang, F. Sun, Z. Wang, D. Zhao, *J. Porous Mater.* **2008**, *15*, 145–150.
- [17] J. C. Jansen, Z. Shan, L. Marchese, W. Zhou, N. v. d. Puil, T. Maschmeyer, *Chem. Commun.* **2001**, 713–714.
- [18] M. S. Hamdy, O. Berg, J. C. Jansen, T. Maschmeyer, J. A. Moulijn, G. Mul, *Chem. Eur. J.* **2006**, *12*, 620–628.
- [19] M. S. Hamdy, G. Mul, *Catal. Sci. Technol.* **2012**, *2*, 1894–1900.
- [20] M. S. Hamdy, O. Berg, J. C. Jansen, T. Maschmeyer, A. Arafat, J. A. Moulijn, G. Mul, *Catal. Today* **2006**, *117*, 337–342.
- [21] M. S. Hamdy, G. Mul, W. Wei, R. Anand, U. Hanefeld, J. C. Jansen, J. A. Moulijn, *Catal. Today* **2005**, *110*, 264–271.
- [22] P. Waller, Z. Shan, L. Marchese, G. Tartaglione, W. Zhou, J. C. Jansen, T. Maschmeyer, *Chem. Eur. J.* **2004**, *10*, 4970–4976.
- [23] J. Wang, J. C. Groen, W. Yue, W. Zhou, M. O. Coppens, *J. Mater. Chem.* **2008**, *18*, 468–474.
- [24] C. C. Aquino, H. O. Pastore, A. F. Masters, T. Maschmeyer, *ChemCatChem* **2011**, *3*, 1759–1762.
- [25] S. Lima, M. M. Antunes, A. Fernandes, M. Pillinger, M. F. Ribeiro, A. A. Valente, *Appl. Catal. A* **2010**, *388*, 141–148.
- [26] M. S. Hamdy, G. Mul, J. C. Jansen, A. Ebaid, Z. Shan, A. R. Overweg, T. Maschmeyer, *Catal. Today* **2005**, *100*, 255–260.
- [27] M. S. Hamdy, G. Mul, G. M. Hamminga, J. A. Moulijn, J. C. Jansen, *Stud. Surf. Sci. Catal.* **2005**, *158*, 1509–1516.
- [28] S. van Donk, A. H. Janssen, J. H. Bitter, K. P. de Jong, *Catal. Rev.* **2003**, *45*, 297–319.
- [29] J. W. Yoon, S. H. Jhung, D. H. Choo, S. J. Lee, K.-Y. Lee, J.-S. Chang, *Appl. Catal. A* **2008**, *337*, 73–77.
- [30] J. Datka, B. Sulikowski, B. Gil, *J. Phys. Chem.* **1996**, *100*, 11242–11245.
- [31] J. Weitkamp, *Solid State Ionics* **2000**, *131*, 175–188.
- [32] D. Goyvaerts, J. A. Martens, P. J. Grobet, P. A. Jacobs, *Stud. Surf. Sci. Catal.* **1991**, *63*, 381–395.
- [33] P. Maki-Arvela, N. Kumar, V. Nieminen, R. Sjöholm, T. Salmi, D. Y. Murzin, *J. Catal.* **2004**, *225*, 155–169.
- [34] A. Ramanathan, D. Klomp, J. A. Peters, U. Hanefeld, *J. Mol. Catal. A: Chem.* **2006**, *260*, 62–69.
- [35] N. Candu, M. Florea, S. M. Coman, V. I. Parvulescu, *Appl. Catal. A* **2011**, *393*, 206–214.
- [36] V. D. Chaube, *Catal. Commun.* **2004**, *5*, 321–326.
- [37] A. Jentys, R. R. Mukti, J. A. Lercher, *J. Phys. Chem. B* **2006**, *110*, 17691–17693.
- [38] N. He, S. Bao, Q. Xu, *Appl. Catal. A* **1998**, *169*, 29–36.
- [39] J. A. Melero, R. Grieken, G. Morales, V. Nuno, *Catal. Commun.* **2004**, *5*, 131–136.

- [40] H. Nur, Z. Ramli, J. Efendi, A. N. A. Rahman, S. Chandren, L. S. Yuan, *Catal. Commun.* **2011**, *12*, 822–825.
- [41] R. Li, W. Fan, J. Ma, K. Xie, *Stud. Surf. Sci. Catal.* **2000**, *129*, 117–120.
- [42] M. E. Sad, C. L. Padró, C. R. Apesteguía, *Catal. Today* **2008**, *133–135*, 720–728.
- [43] B. Thomas, B. B. Das, S. Sugunan, *Microporous Mesoporous Mater.* **2006**, *95*, 329–338.
- [44] W. Liang, Y. Jin, Z. Yu, Z. Wang, B. Han, M. He, E. Min, *Zeolites* **1996**, *17*, 297–303.
- [45] X. Dong, Y. Song, W. Lin, *Catal. Commun.* **2007**, *8*, 539–542.
- [46] D. Mores, J. Kornatowski, U. Olsbye, B. M. Weckhuysen, *Chem. Eur. J.* **2011**, *17*, 2874–2884.

Received: June 13, 2013

Published online on August 12, 2013